Antiviral Research 169 (2019) 104536

Contents lists available at ScienceDirect

Antiviral Research

journal homepage: www.elsevier.com/locate/antiviral

Structure of the yellow fever NS5 protein reveals conserved drug targets shared among flaviviruses

Anna Dubankova, Evzen Boura*

Institute of Organic Chemistry and Biochemistry of the Czech Academy of Sciences, Flemingovo Nam. 2, 166 10, Prague 6, Czech Republic

ARTICLE INFO

Keywords:
RNA
Polymerase
Crystal structure
Flavivirus
Yellow fever
Drug design

ABSTRACT

Yellow fever virus (YFV) is responsible for devastating outbreaks of Yellow fever (YF) in humans and is associated with high mortality rates. Recent large epidemics and epizootics and exponential increases in the numbers of YF cases in humans and non-human primates highlight the increasing threat YFV poses, despite the availability of an effective YFV vaccine. YFV is the first human virus discovered, but the structures of several of the viral proteins remain poorly understood. Here we report the structure of the full-length NS5 protein, a key enzyme for the replication of flaviviruses that contains both a methyltransferase domain and an RNA dependent RNA polymerase domain, at 3.1 Å resolution. The viral polymerase adopts right-hand fold, demonstrating the similarities of the Yellow fever, Dengue and Zika polymerases. Together this data suggests NS5 as a prime and ideal target for the design of pan-flavivirus inhibitors.

1. Introduction

Yellow fever virus (YFV) is a mosquito-borne virus (Epelboin et al., 2017), along with several other flaviviruses such as the Zika virus (ZIKV) and Dengue virus. The population of the mosquito *Aedes aegypti*, which is the major mosquito species responsible for transmission of these viruses, is growing due to global climatic changes (Monaghan et al., 2018). As a result, flaviviruses are becoming a global threat to mankind as documented by the recent Zika (Abushouk et al., 2016) and Yellow Fever (YF) outbreaks (Blake and Garcia-Blanco, 2014; Couto-Lima et al., 2017). The outbreaks are moreover associated with high mortality (YF) or cause microcephaly in infants and Guillain-Barré syndrome (ZIKV) in some patients (Krauer et al., 2017). Unfortunately, despite the availability of an effective YFV vaccine, large epidemics and epizootics of YF were recently reported in Brazil and Angola with exponential increases in the numbers of YF cases in humans and non-human primates (Barrett, 2018). These outbreaks indicate that both an effective antiviral vaccine and antiviral cure are important.

YFV and its transmission by mosquitoes was discovered in 1900 (Reed et al., 1900) and significant progress in understanding this virus has been made since then. For instance, the structure of the YFV capsid was solved by cryo-electron microscopy (Zhang et al., 2003) and the crystal structure of NS3 helicase is also available (Wu et al., 2005). Despite these advances, the structures of several of the viral proteins remain poorly understood (Douam and Ploss, 2018). Of these, the NS5 protein is a key enzyme for the replication of flaviviruses because it contains an N-terminal methyltransferase (MTase) domain and a C-terminal RNA dependent RNA polymerase (RdRp) domain (Fig. 1A) (Selisko et al., 2018). The MTase domain has two enzymatic activities: it is responsible for guanine-N7 and nucleoside-2′-O methylation (Coutard et al., 2017; Dong et al., 2010; Hercik et al., 2017a), both of which increase the stability of newly synthesized RNA by preventing degradation by 5′–3′ exoribonucleases. RNA methylation also helps the virus to avoid the innate immunity (Hyde and Diamond, 2015) as non-methylated RNA is recognized by the innate immunity factor Ifit1 (IFN-induced RNA-binding protein) and its translation inhibited. The RdRp domain is essential for replication of viral RNA because its enzymatic activity cannot be replaced by any host enzyme. Therefore, both domains are indispensable for flaviviral replication making the NS5 enzyme a prime target for drug discovery (Lim et al., 2015).

For some flaviviruses including Zika and Dengue the structure of the NS5 protein was reported (Duan et al., 2017; Godoy et al., 2017; Upadhyay et al., 2017; Zhao et al., 2015, 2017). In the case of Yellow fever, however, only the structure of the methyltransferase domain was described (Geiss et al., 2009). Here, we describe the crystal structure of the full-length Yellow fever NS5 enzyme at 3.1 Å resolution. It reveals the right-hand fold typical for viral polymerases and highlights conserved regions between Yellow fever, Dengue and Zika, thus providing critical information for structure-aided drug design.

* Corresponding author.
E-mail address: boura@uochb.cas.cz (E. Boura).

https://doi.org/10.1016/j.antiviral.2019.104536
Received 16 April 2019; Received in revised form 7 June 2019; Accepted 12 June 2019
Available online 13 June 2019

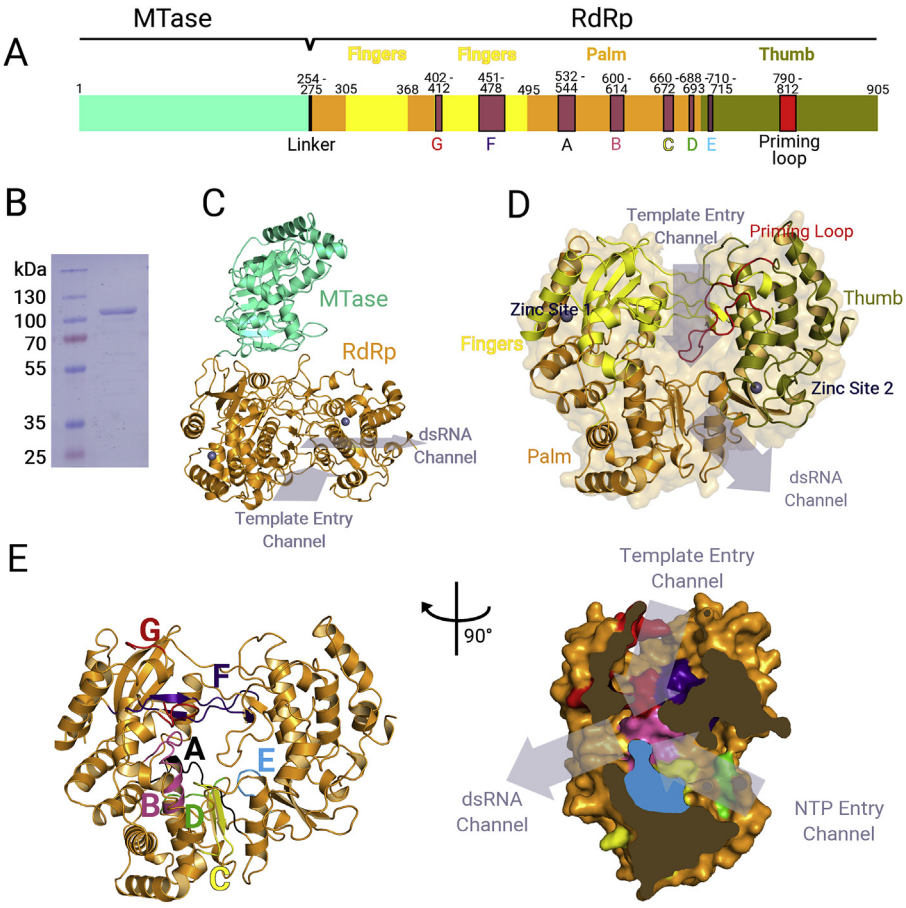

Fig. 1. Structure of the full-length YF NS5 protein.
A. YFV NS5 is composed of the MTase domain and the RdRp. Three subdomains and seven motifs (A-G) occur in the RdRp domain.
B. Recombinant YFV NS5 FL protein was used for all experiments (99% pure based on SDS PAGE analysis).
C. The structure of the YF FL NS5 protein in ribbon representation. The MTase domain is shown in cyan and the RdRp domain is shown in orange.
D. Structure of the RdRp domain. The template entry, dsRNA and NTP entry channels as well as the fingers, palm and thumb subdomains are highlighted.
E. Positions of the seven motifs of the RdRp domain. The template entry channel contains the F and G motifs, while the NTP entry channel contains the B, C, D and E motifs.

2. Results

We aimed to obtain the crystal structure of the Yellow fever polymerase, as understanding the structural conservation and differences across flaviviruses will help in rational drug design. We expressed the full-length NS5 protein from the Yellow fever strain 17D vaccine in *E. coli* and optimized the purification protocol to obtain highly pure protein (Fig. 1B). After crystal optimization, we obtained crystals that diffracted to ~3 Å and were able to collect a complete dataset at 3.1 Å resolution. The crystals contained two molecules of the NS5 enzyme in the asymmetric unit and we solved the structure by molecular replacement using the methyltransferase domain and a homology model of the RdRp domain (described in detail in M&M section). This made it possible to trace the entire polypeptide chain except for the very first five residues at the N-terminus, the very last eleven residues at the C-terminus, and a disordered loop between Ile410 and Glu418. The two molecules in the asymmetric unit are virtually identical and superimpose with an RMSD of 0.29 Å (SI Fig. 1). The final model was refined to R_{work} = 22.07% and R_{free} = 27.00% (Table 1).

The overall structure can be divided into an RdRp domain and a methyltransferase domain that is stacked on the fingers and F motif of the RdRp domain (Fig. 1C). The MTase domain consists of nine helices and nine β-strands that forms a classic α/β/α sandwich structure (Byszewska et al., 2014), which form the GTP and SAM binding sites. We clearly observed the electron density of a ligand in the SAM pocket (SI Fig. 2) and we modeled the SAH (S-adenosylhomocysteine) into the map. However, the observed electron density probably corresponds to a mixture of SAH and SAM (S-adenosylmethionine) since both these ligands are present in *E. coli*. and they co-purify with the recombinant protein. Because a high resolution structure of YF MTase domain is already available (Geiss et al., 2009) and we didn't observe any discrepancies (RMSD of 0.94 Å, SI Fig. 3) we will not describe the structure of the MTase domain in detail here.

The RdRp domain has a right-hand fold as expected (Fig. 1) with three channels (template entry, dsRNA and NTP entry channel) and can be divided into fingers, palm and thumb subdomains (Fig. 1C). The fingers subdomain is composed of two regions, the first of which is

Table 1
Statistics of crystallographic data collection and refinement.

Data collection	
Space group	$P2_12_12_1$
Cell dimension (Å)	a = 108.3 b = 142.1 , c = 152.2
X-ray source	BESSY ID 14-2
Resolution (Å)	47.8 - 3.0 (3.11 - 3.00)
Unique reflections	47,148 (4576)
I/σ (I)	9.91 (1.13)[a]
Wavelength (Å)	0.9184
Multiplicity	8.3 (8.5)
Completeness (%)	99.19 (97.65)
R-pim, %	8.1 (68.7)
$CC_{1/2}$	0.994 (0.419)
CC*	0.999 (0.769)
Refinement	
R-work, %	22.07 (32.22)
R-free, %	27.00 (33.90)
RMS(bonds), °	0.002
RMS(angles), Å	0.51
Ramachandran (outliers/favored) (%)	0.0%/97.8%

Numbers in parentheses refer to the highest resolution shell.
[a] I/σ (I) = 2 at 3.1 Å.

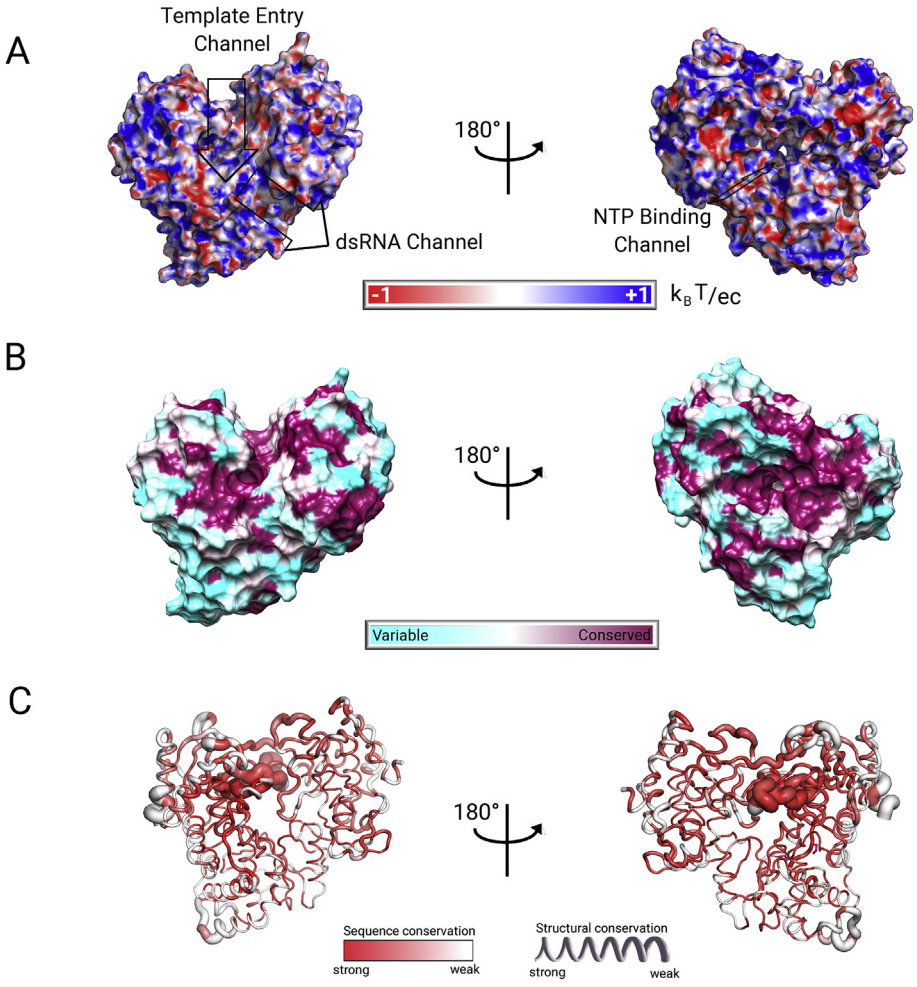

Fig. 2. Surface and structural analysis of YF RdRp.
A. The surface of the template entry channel is positively charged and, optimized to bind the RNA substrate.
B. Surface representation of the YF RdRp domain colored according to sequence conservation (cyan: not conserved, dark magenta: conserved). This shows the highly conserved protein core and variable periphery.
C. Sausage representation based on a combination of sequence and structural alignments of Flaviviral NS5 proteins reveals structural differences in regions in which the sequence is conserved. Structures used for this alignment are: WNV (2hcn, 2hfz), DENV(2j7u, 3vws, 4v0q, 4v0r, 5ccv, 5dto, 5iq6, 5k5m), JEV (4hdg, 4k6m, 4mtp), ZIKV (5m2x, 5tfr, 5tmh, 5u0b, 5u0c, 5u04, 5wz3).

located in helices α11 - 14 and sheets β10 - 12 (residue 305–368) and the second of which is located in helices α16 - 20 and sheets β13 - 14 (residues 402–495). In contrast, the palm subdomain is spread throughout the RdRp. It consists of three regions, helix α10 (residues 275–305), helices α15 – 16 (residues 368–402) and helices α21 – 31 together with beta sheets β16 – 20 (residues 495–720) and forms the core of the RdRp. The thumb subdomain is composed of the C terminus of RdRp (helices α32 – 40 and beta sheets β21 - 22, residues 722–905) and together with the palm subdomain form the dsRNA channel.

The seven catalytic motifs (A - G), that are present in every viral RdRp (Lu and Gong, 2017), could also be detected in the YF RdRp domain. Motif A is located in helix α23 and contains the catalytically important aspartate residues Asp535 and Asp541. Motif B contains highly conserved Ser603 and Gly604 residues. The sidechain of Ser603 interacts with the 2′-hydroxyl group of the ribose ring during active side closure (Appleby et al., 2015) while motifs C and E, located in β18 and 19 respectively in a loop between helix α31 and sheet β20, interact with the backbone of the RNA product. Motif D that is localized adjacent to helix α30 is important for the active site closure by the conserved lysine residue Lys359 (Yang et al., 2012). Motif F consists of three beta sheets (β13 – 15) and connecting loops, it is located at the top of the NTP entry channel and its primary function is to bind the NTP nucleotide. Importantly, it contains a conserved phenylalanine residue Phe466 at the interface of the RdRp and MTase domains. Motif G contacts the backbone of the template RNA in other non-flaviviral RdRp enzymes (Appleby et al., 2015; Gong et al., 2013; Gong and Peersen, 2010) is located in a loop located between α16 and 17 (Fig. 1A).

The template entry channel is surrounded by the fingers and thumb subdomains with the priming loop above. It also contains motifs G and F, which interact with the RNA template. It is followed by the dsRNA channel which forms a ~45° angle to the template entry channel. The dsRNA channel is formed mainly by the palm subdomain and motifs C and E. The NTP channel is localized between the template and dsRNA channels and contains the A, B and D motifs (Fig. 1E). Surface electrostatic potential analysis reveals that the channels are positively charged (Fig. 2) which is essential for RNA binding. The priming loop (Fig. 1D in red) is localized above the interface of the three channels. Its purpose is to properly position nucleotides for RNA polymerization (Ng et al., 2008). Based on structural analysis of the HCV polymerase it was proposed that a stacking interaction occurs between a residue in the priming loop (tyrosine in the case of HCV) and the initiating nucleotide (Butcher et al., 2001). In Zika this role was proposed to be played by the highly conserved tryptophan residue Trp797 (Zhao et al., 2017) which corresponds to Trp799 in YF. In a computational (QM/MM devised) model of Zika NS5 with RNA, the Trp797 is positioned above the base suggesting a T-shaped stacking interaction (Sebera et al., 2018).

Two zinc binding sites occur in the fingers and thumb subdomains of the RdRp (Fig. 3). These are also present in every flaviviral RdRp structure solved so far. The first zinc atom is coordinated by Cys448, Cys451, His443 and Glu439 and the second zinc binding site is formed by Cys732, Cys851, His716 and His718. A glutamate residue in a zinc binding site is somewhat unusual, however, this glutamate and other residues forming the first zinc binding site are absolutely conserved among NS5 proteins from YFV, ZIKV, DEN, and WNV (Fig. 3C). The second zinc binding site is partially conserved: Cys732, Cys851, His716 are conserved, while His718 is replaced by an asparagine residue in Zika and by a threonine residue in WNV (Fig. 3C). As a consequence, the zinc ion is coordinated by water molecule instead of a histidine at

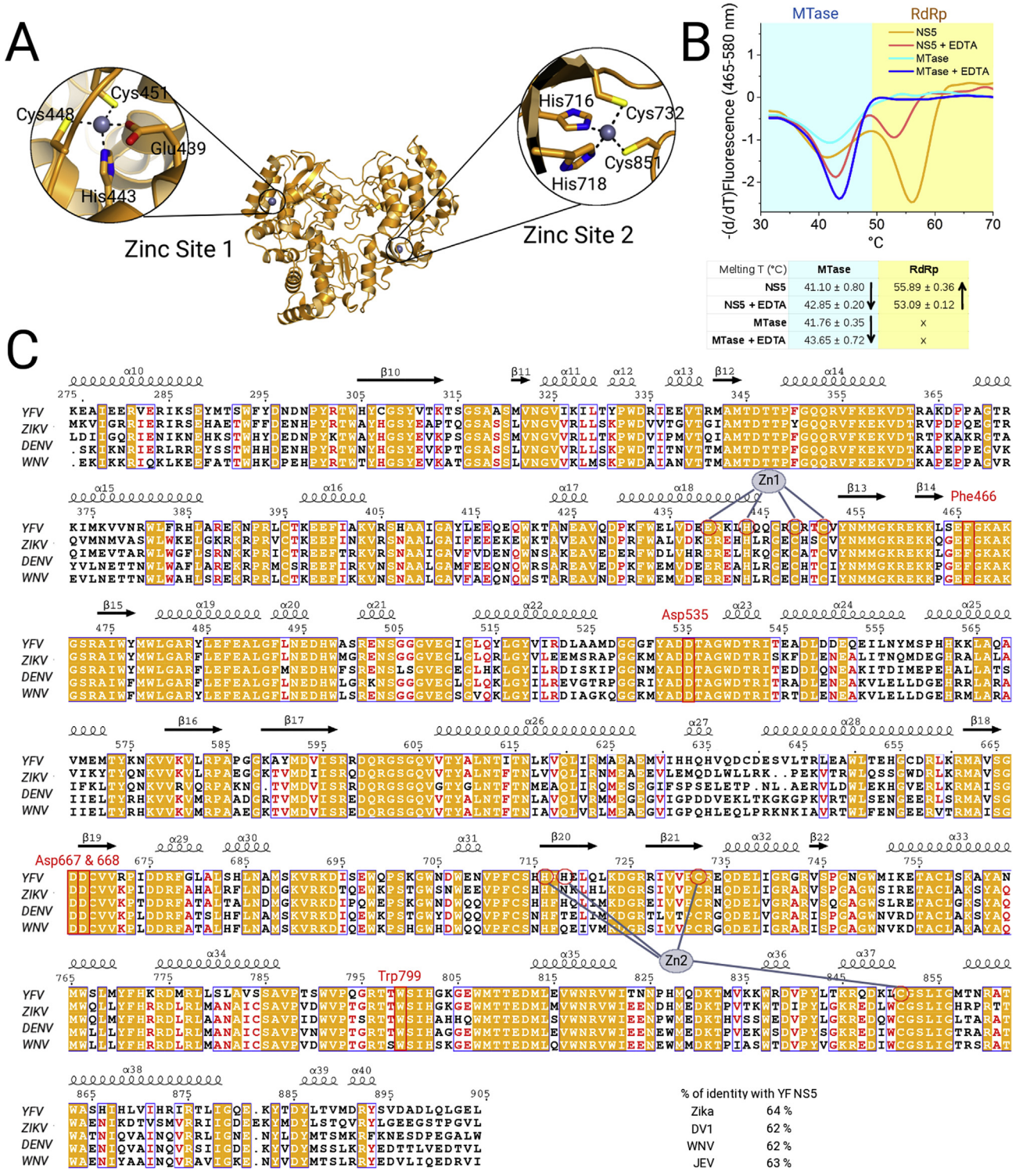

Fig. 3. Localization of the zinc binding sites in the RdRp domain.

A. Zoomed view of the two YF RdRp zinc binding sites. The first zinc atom is coordinated by Glu439, His443, Cys448 and Cys451, while the second one by His716, His718, Cys732 and Cys851.

B. The zinc biding sites stabilize the NS5 protein. Addition of the chelating agent EDTA decreases the thermal stability of the full length NS5 protein but not that of the MTase domain.

C. Sausage representation based on a combination of sequence and structural alignments of Flaviviral NS5 proteins reveals structural differences in regions in which the sequence is conserved. Structures used for this alignment were from WNV (2hcn, 2hfz), DENV(2j7u, 3vws, 4v0q, 4v0r, 5ccv, 5dto, 5iq6, 5k5m), JEV(4hdg, 4k6m, 4mtp), and ZIKV (5m2x, 5tfr, 5tmh, 5u0b, 5u0c, 5u04, 5wz3). In the lower right panel is shown percentage of individual mentioned sequences identity with yellow fever NS5 sequence.

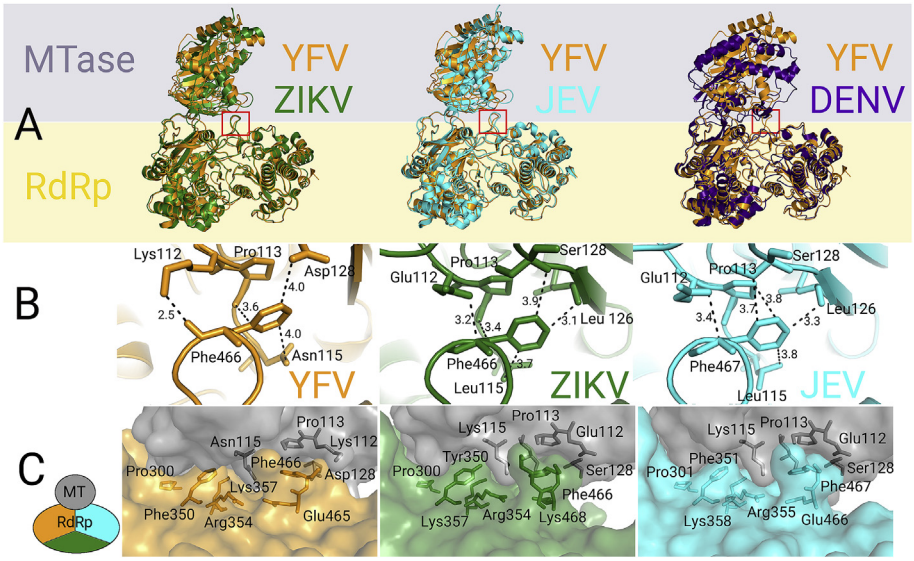

Fig. 4. The MTase:RdRp interface.
A. Structures of full length flaviviral NS5 proteins were superimposed on the structure of YF NS5 based on the RdRp domain. This revealed that the domain orientation is conserved in Yellow fever, Zika and Japanese encephalitis virus RdRp but not in Dengue RdRp.
B. The conserved residues Phe466 and Pro113 define the MTase:RdRp interface.
C. Detail of RdRp MTase interface. MTase is shown in gray color. The color of RdRp is colored depending on viral origin (YFV – yellow, ZIKV – forest green, JEV – cyan).

this position (Duan et al., 2017). The zinc binding sites stabilize the RdRp domain, as the melting temperature (T_m) of the RdRp domain drops from 55.9 °C and to 53.1 °C in the presence of the chelating agent EDTA (Fig. 3B).

For Zika NS5 enzyme it was previously shown that the MTase domain activates the RdRp domain (Zhao et al., 2017). The Zika MTase domain stabilizes motif F in the RdRp domain using a mechanism in which the conserved phenylalanine residue Phe466 stacks against a pocket on the surface of the MTase domain formed by Leu115, Leu126, Pro113 (Fig. 4, and Fig. SI) (Fig. 4 for the electron density maps). This inter-domain interface is further stabilized by a hydrogen bond between the sidechain of Glu112 and the backbone of motif F (Rusanov et al., 2018). We superimposed the structure of the YF NS5 with other known full-length flaviviral NS5 proteins (Fig. 4A) and this comparison revealed that the MTase:RdRp interface is conserved among YF, Zika (PDB: 5tfr) (Upadhyay et al., 2017) and JEV (Japanese encephalitis virus, PDB:4k6m) (Lu and Gong, 2013). In contrast, the structure of Dengue NS5 (PDB: 4v0q) (Zhao et al., 2015) maintains an F motif that is disordered. Moreover, the residues of the MTase domain adjacent to the conserved residue Pro113, which form the patch which interacts with Phe466, are not conserved, although, the mode of binding is conserved (Fig. 4). In case of YF, Lys112 forms a hydrogen bond with the backbone of Phe466. However, the aromatic ring of Phe466 residue is always stacked against the pyrrolidine ring of Pro113, which is also seen in the structures of the full-length Zika and JEV NS5 enzymes, suggesting that the interaction of Phe466 with Pro113 is the key feature of the MTase:RdRp interface (Fig. 4B and C).

3. Discussion

YF killed hundreds of thousands of people in the 18th and 19th centuries and, according to the World Health Organization, it still causes 84,000–170,000 severe cases and 29,000–60,000 deaths annually despite extensive vaccination. The primary target for antiviral therapy is the NS5 enzyme because both of its domains - the RdRp and MTase - are together crucial for viral replication. As a result, inhibitors of NS5 enzyme are in continual development (Eyer et al., 2016; Hercik et al., 2017b; Stephen et al., 2016). Despite this, the structure of the full-length YF NS5 protein was until now unavailable despite the importance of YF for global human health. Structure-guided inhibitor design is being used with increasing frequency and the lack of a structure of the YF NS5 has made a significant impediment for rational drug design specific to YF. Here we filled this gap by solving the structure of YF NS5 enzyme at 3.1 Å resolution.

This structure reveals the MTase:RdRp interface, which is conserved in the structures of the YF, Zika, and JEV NS5 enzymes but not in the structure of Dengue NS5. The two key residues forming this interface are Pro113 in the MTase domain and Phe446 in the F motif of the RdRp domain. These residues are also conserved in Dengue NS5 enzyme, although the F motif in the structure of the full-length Dengue NS5 enzyme is disordered. The different orientation of the MTase domain in the case of the Dengue enzyme could be a crystal packing artifact, however, that seems unlikely because another structure of the Dengue NS5 enzyme with an inhibitor bound has the same orientation of the MTase and RdRp domain (Lim et al., 2016). It is well established, however, that by stabilizing the F motif, the MTase domain activates the RdRp domain. Interestingly, our structure reveals that the residue Glu111, a neighbor of Lys112 which is involved in F motif stabilization, also forms a hydrogen bond with the sugar hydroxyl group of SAH (Fig. 5). This suggests that not only the MTase domain but also the RdRp domain could influence the enzymatic activity of the MTase domain. Alternatively, it could mean that only ligand bound MTase domain can activate the RdRp domain. Unfortunately, this hypothesis is hard to test because full-length NS5 enzyme without ligand cannot be prepared in bacterial nor eukaryotic expression systems. Another suggested mechanism of an interplay between the MTase and RdRp polymerase is the GTP depended multimerization of the Zika full-length NS5 which could be important for the regulation of the RdRp domain by the MTase domain (Ferrero et al., 2019). Also the role of the membrane remains to be better defined as membranes were suggested to recruit viral polymerases (Dubankova et al., 2017; Hsu et al., 2010) and such a recruitment could initiate the polymerization.

Taken together, this structure revealed several conserved regions among flaviviral polymerases including the catalytic aspartate residues Asp535, Asp667 and Asp668 which coordinate magnesium cations during polymerization reaction, the conserved tryptophan Trp797 within the priming loop and the highly conserved first zinc binding site in the fingers subdomain but not the second zinc binding site (Fig. 6). Our structural analysis suggests that a compound targeting any of these sites would likely be active against multiple flaviviruses.

4. Materials and methods

Protein expression and purification – Artificial codon optimized gene encoding YFV NS5 enzyme (strain 17D vaccine, UniProtKB - P03314) was commercially synthesized (Invitrogen) and cloned into a pSUMO vector using Gibson assembly method. The resulting sequence encoded for a His_{8x}SUMO-NS5 fusion protein. The protein was expressed and

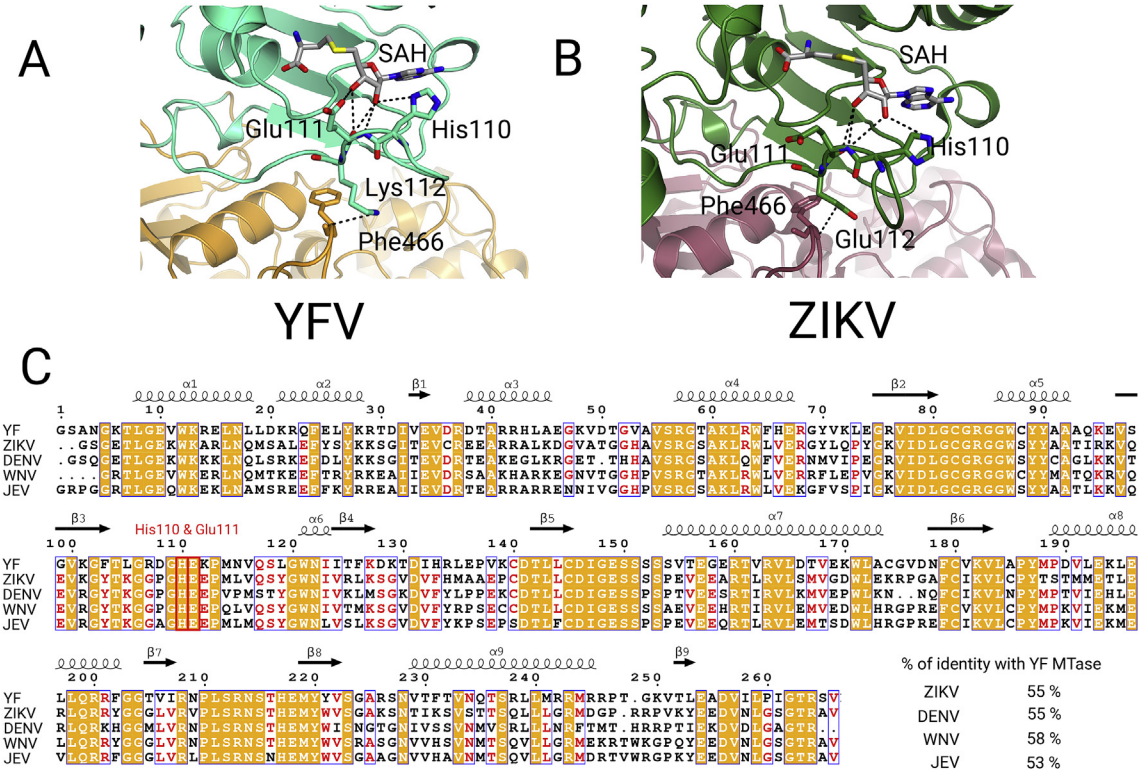

Fig. 5. Loop of the MTase domain contains both, residues coordinating the SAH ligand and residues stabilizing the F motif of the RdRp domain.
A. Detailed view showing the hydrogen bond of MTase localized residue Lys112 to the conserved residue Phe466 of the F motif and the neighboring residues Glu111 and His110 stabilizing the SAH ligand.
B. Residue Glu112 fulfills the same function as YFV Lys112 in other flaviviral polymerases.
C. Sequence alignment illustrating conservation of key residues except of Lys112 that is replaced by Glu112 in other flaviviruses, although, Glu112 fulfills the same structural function.

purified using our standard protocols with some modifications (Baumlova et al., 2014). Briefly, it was expressed in *E. coli* strain BL21 Star in autoinduction ZY media supplemented with 50 μM $ZnSO_4$. The bacteria were lysed using Emulsiflex C3 (Avestin) in the lysis buffer (50 mM Tris pH = 8, 500 mM NaCl, 20 mM imidazole, 3 mM βME). After lysis the protein was immobilized on NiNTA Agarose resin (Machery-Nagel) and extensively washed with the lysis buffer and eluted with the lysis buffer supplemented with 300 mM imidazole. The His_{8x}SUMO solubilisation tag was cleaved by the Ulp1 protease (1.0 mg per 20 mg of YF NS5) at 4 °C overnight. The YF NS5 was further purified by size exclusion chromatography in SEC buffer (20 mM Tris pH 8, 1 M NaCl, 3 mM βME, 10% glycerol). Finally, the protein was concentrated to 6 mg/ml and stored in −80 °C until needed.

Crystallization, data analysis and refinement – Crystals grew in sitting drops consisting of 300 nl of the protein and the well solution (80 mM Tris pH = 8.5, 1.92M $(NH_4)_2SO_4$, 20% (v/v) glycerol) in about a week. Upon harvest were the crystals flash frozen in liquid nitrogen and diffraction data were collected at the 14.2 BESSY beamline in HZB synchrotron facility (Mueller et al., 2012). The crystals diffracted to 3 Å and belonged to the orthorhombic $P2_12_12_1$ space group.

The diffraction data were collected from a single frozen crystal at 100 K and processed using XDS (Kabsch, 2010) within the XDSAPP GUI (Krug et al., 2012). The data were cut at 3 Å where the correlation coefficient $C_{1/2}$ = 0.4. The structure was solved by molecular replacement using two models, the YF methyltransferase domain (pdb code 3EVA) (Geiss et al., 2009) and a homology model of the RdRp domain based on the structure of Japanese encephalitis virus NS5 (pdb code 4K6M) (Lu and Gong, 2013). The structure was further build and refined manually using Phenix (Adams et al., 2010) and Coot (Emsley et al., 2010) to R_{work} = 22.07% and R_{free} = 27.03% and good geometry as summarized in Table 1. Structural figures were generated by PyMol (Schrodinger).

Thermal Shift Assay - The thermal shift assay was run in presence of 1 μM protein, 5000 x diluted SYPRO Orange Protein Gel Stain and 20 mM Tris pH 7.4, 40 mM NaCl, 10 mM βME, 20 mM $MgCl_2$ (and 100 mM EDTA). The mixture was continually heated from 25 to 95 °C in 20 min. The fluorescence signal was measured in a ROCHE LightCycler® 480.

Primary structure alignments were rendered and analyzed by ESPript 3.0 (Robert and Gouet, 2014).

Accession numbers

Atomic coordinates and structure factors have been deposited in the Protein Data Bank with accession codes 6QSN.

Author contributions

AD performed all experiments and wrote the manuscript. EB conceived and supervised the study, analyzed the data, and wrote the manuscript.

Conflicts of interest

The authors declare that they have no conflict of interest.

Funding

The work was supported from European Regional Development Fund; OP RDE; Project: “Chemical biology for drugging undruggable targets (ChemBioDrug)” (No. CZ.02.1.01/0.0/0.0/16_019/0000729) and by the Academy of Sciences Czech Republic (RVO: 61388963).

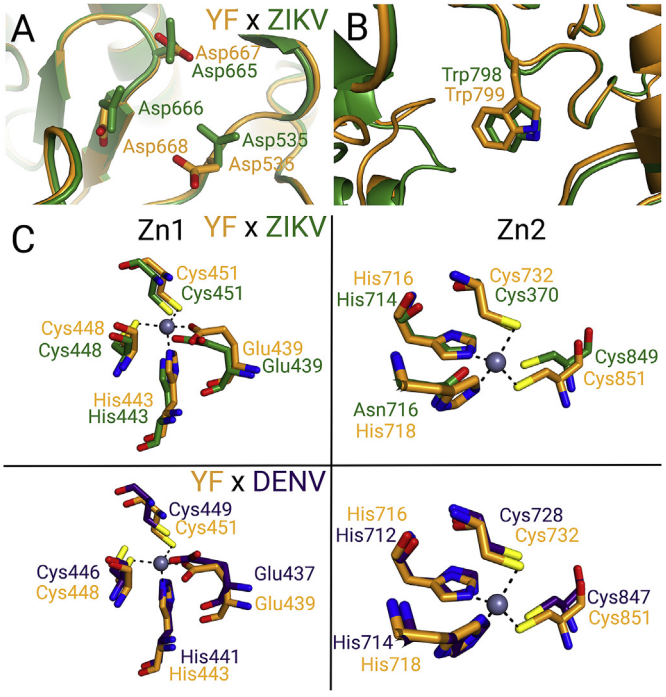

Fig. 6. Superposition of selected motifs of YF, ZIKV or DENV polymerases.
A. YF and ZIKV superposition illustrates the conservation of the Mg^{2+} binding Asp trinity.
B. Residue Trp799 in the priming loop is highly conserved.
C. Superposition of YF and ZIKV or DENV zinc fingers 1 and 2 (Zn1 and Zn2). Zn1 is fully conserved compared to zinc finger in position 2, where His 718 is conserved in YF and DENV, but not in ZIKV RdRp.

Acknowledgements

We thank HZB for the allocation of synchrotron radiation beamtime. We are grateful to Dr. Perta Krafcikova for the gift of the recombinant MTase domain and to David Murray, Tom Leonard and Edward Curtis for critical reading of the manuscript.

Appendix A. Supplementary data

Supplementary data to this article can be found online at https://doi.org/10.1016/j.antiviral.2019.104536.

References

Abushouk, A.I., Negida, A., Ahmed, H., 2016. An updated review of Zika virus. J. Clin. Virol.Off. Publ. Pan-Am. Soc. Clin. Virol. 84, 53–58.
Adams, P.D., Afonine, P.V., Bunkoczi, G., Chen, V.B., Davis, I.W., Echols, N., Headd, J.J., Hung, L.W., Kapral, G.J., Grosse-Kunstleve, R.W., McCoy, A.J., Moriarty, N.W., Oeffner, R., Read, R.J., Richardson, D.C., Richardson, J.S., Terwilliger, T.C., Zwart, P.H., 2010. PHENIX: a comprehensive Python-based system for macromolecular structure solution. Acta Crystallogr. Sect. D Biol. Crystallogr. 66, 213–221.
Appleby, T.C., Perry, J.K., Murakami, E., Barauskas, O., Feng, J., Cho, A., Fox third ed, D., Wetmore, D.R., McGrath, M.E., Ray, A.S., Sofia, M.J., Swaminathan, S., Edwards, T.E., 2015. Viral replication. Structural basis for RNA replication by the hepatitis C virus polymerase. Science 347, 771–775.
Barrett, A.D.T., 2018. The reemergence of yellow fever. Science 361, 847–848.
Baumlova, A., Chalupska, D., Rozycki, B., Jovic, M., Wisniewski, E., Klima, M., Dubankova, A., Kloer, D.P., Nencka, R., Balla, T., Boura, E., 2014. The crystal structure of the phosphatidylinositol 4-kinase IIalpha. EMBO Rep. 15, 1085–1092.
Blake, L.E., Garcia-Blanco, M.A., 2014. Human genetic variation and yellow fever mortality during 19th century. U.S. epidemics. mBio 5 e01253-01214.
Butcher, S.J., Grimes, J.M., Makeyev, E.V., Bamford, D.H., Stuart, D.I., 2001. A mechanism for initiating RNA-dependent RNA polymerization. Nature 410, 235–240.
Byszewska, M., Smietanski, M., Purta, E., Bujnicki, J.M., 2014. RNA methyltransferases involved in 5' cap biosynthesis. RNA Biol. 11, 1597–1607.
Coutard, B., Barral, K., Lichiere, J., Selisko, B., Martin, B., Aouadi, W., Lombardia, M.O., Debart, F., Vasseur, J.J., Guillemot, J.C., Canard, B., Decroly, E., 2017. Zika virus methyltransferase: structure and functions for drug design perspectives. J. Virol. 91.
Couto-Lima, D., Madec, Y., Bersot, M.I., Campos, S.S., Motta, M.A., Santos, F.B.D., Vazeille, M., Vasconcelos, P., Lourenco-de-Oliveira, R., Failloux, A.B., 2017. Potential risk of re-emergence of urban transmission of Yellow Fever virus in Brazil facilitated by competent Aedes populations. Sci. Rep. 7, 4848.
Dong, H., Chang, D.C., Xie, X., Toh, Y.X., Chung, K.Y., Zou, G., Lescar, J., Lim, S.P., Shi, P.Y., 2010. Biochemical and genetic characterization of dengue virus methyltransferase. Virology 405, 568–578.
Douam, F., Ploss, A., 2018. Yellow fever virus: knowledge gaps impeding the fight against an old foe. Trends Microbiol. 26, 913–928.
Duan, W., Song, H., Wang, H., Chai, Y., Su, C., Qi, J., Shi, Y., Gao, G.F., 2017. The crystal structure of Zika virus NS5 reveals conserved drug targets. EMBO J. 36, 919–933.
Dubankova, A., Humpolickova, J., Klima, M., Boura, E., 2017. Negative charge and membrane-tethered viral 3B cooperate to recruit viral RNA dependent RNA polymerase 3D (pol). Sci. Rep. 7, 17309.
Emsley, P., Lohkamp, B., Scott, W.G., Cowtan, K., 2010. Features and development of Coot. Acta crystallographica. Acta Crystallogr. Sect. D Biol. Crystallogr. 66, 486–501.
Epelboin, Y., Talaga, S., Epelboin, L., Dusfour, I., 2017. Zika virus: an updated review of competent or naturally infected mosquitoes. PLoS Neglected Trop. Dis. 11, e0005933.
Eyer, L., Nencka, R., Huvarova, I., Palus, M., Joao Alves, M., Gould, E.A., De Clercq, E., Ruzek, D., 2016. Nucleoside inhibitors of Zika virus. J. Infect. Dis. 214, 707–711.
Ferrero, D.S., Ruiz-Arroyo, V.M., Soler, N., Uson, I., Guarne, A., Verdaguer, N., 2019. Supramolecular arrangement of the full-length Zika virus NS5. PLoS Pathog. 15, e1007656.
Geiss, B.J., Thompson, A.A., Andrews, A.J., Sons, R.L., Gari, H.H., Keenan, S.M., Peersen, O.B., 2009. Analysis of flavivirus NS5 methyltransferase cap binding. J. Mol. Biol. 385, 1643–1654.
Godoy, A.S., Lima, G.M., Oliveira, K.I., Torres, N.U., Maluf, F.V., Guido, R.V., Oliva, G., 2017. Crystal structure of Zika virus NS5 RNA-dependent RNA polymerase. Nat. Commun. 8, 14764.
Gong, P., Kortus, M.G., Nix, J.C., Davis, R.E., Peersen, O.B., 2013. Structures of coxsackievirus, rhinovirus, and poliovirus polymerase elongation complexes solved by engineering RNA mediated crystal contacts. PLoS One 8, e60272.
Gong, P., Peersen, O.B., 2010. Structural basis for active site closure by the poliovirus RNA-dependent RNA polymerase. In: Proceedings of the National Academy of Sciences of the United States of America. vol. 107. pp. 22505–22510.
Hercik, K., Brynda, J., Nencka, R., Boura, E., 2017a. Structural basis of Zika virus methyltransferase inhibition by sinefungin. Arch. Virol. 162, 2091–2096.
Hercik, K., Kozak, J., Sala, M., Dejmek, M., Hrebabecky, H., Zbornikova, E., Smola, M., Ruzek, D., Nencka, R., Boura, E., 2017b. Adenosine triphosphate analogs can efficiently inhibit the Zika virus RNA-dependent RNA polymerase. Antivir. Res. 137, 131–133.
Hsu, N.Y., Ilnytska, O., Belov, G., Santiana, M., Chen, Y.H., Takvorian, P.M., Pau, C., van der Schaar, H., Kaushik-Basu, N., Balla, T., Cameron, C.E., Ehrenfeld, E., van Kuppeveld, F.J., Altan-Bonnet, N., 2010. Viral reorganization of the secretory pathway generates distinct organelles for RNA replication. Cell 141, 799–811.
Hyde, J.L., Diamond, M.S., 2015. Innate immune restriction and antagonism of viral RNA lacking 2-O methylation. Virology 479–480, 66–74.
Kabsch, W., 2010. Xds. Acta crystallographica. Acta Crystallogr. Sect. D Biol. Crystallogr. 66, 125–132.
Krauer, F., Riesen, M., Reveiz, L., Oladapo, O.T., Martinez-Vega, R., Porgo, T.V., Haefliger, A., Broutet, N.J., Low, N., Grp, W.Z.C.W., 2017. Zika virus infection as a cause of congenital brain abnormalities and guillain-barre syndrome: systematic review. PLoS Med. 14.
Krug, M., Weiss, M.S., Heinemann, U., Mueller, U., 2012. XDSAPP: a graphical user interface for the convenient processing of diffraction data using XDS. J. Appl. Crystallogr. 45, 568–572.
Lim, S.P., Noble, C.G., Seh, C.C., Soh, T.S., El Sahili, A., Chan, G.K., Lescar, J., Arora, R., Benson, T., Nilar, S., Manjunatha, U., Wan, K.F., Dong, H., Xie, X., Shi, P.Y., Yokokawa, F., 2016. Potent allosteric dengue virus NS5 polymerase inhibitors: mechanism of action and resistance profiling. PLoS Pathog. 12, e1005737.
Lim, S.P., Noble, C.G., Shi, P.Y., 2015. The dengue virus NS5 protein as a target for drug discovery. Antivir. Res. 119, 57–67.
Lu, G., Gong, P., 2013. Crystal Structure of the full-length Japanese encephalitis virus NS5 reveals a conserved methyltransferase-polymerase interface. PLoS Pathog. 9, e1003549.
Lu, G., Gong, P., 2017. A structural view of the RNA-dependent RNA polymerases from the Flavivirus genus. Virus Res. 234, 34–43.
Monaghan, A.J., Sampson, K.M., Steinhoff, D.F., Ernst, K.C., Ebi, K.L., Jones, B., Hayden, M.H., 2018. The potential impacts of 21st century climatic and population changes on human exposure to the virus vector mosquito Aedes aegypti. Clim. Change 146, 487–500.
Mueller, U., Darowski, N., Fuchs, M.R., Forster, R., Hellmig, M., Paithankar, K.S., Puhringer, S., Steffien, M., Zocher, G., Weiss, M.S., 2012. Facilities for macromolecular crystallography at the helmholtz-zentrum berlin. J. Synchrotron Radiat. 19, 442–449.
Ng, K.K., Arnold, J.J., Cameron, C.E., 2008. Structure-function relationships among RNA-dependent RNA polymerases. Curr. Top. Microbiol. Immunol. 320, 137–156.
Reed, W., Carroll, J., Agramonte, A., Lazear, J.W., 1900. The etiology of yellow fever-A preliminary note. Public Health Pap Rep 26, 37–53.
Robert, X., Gouet, P., 2014. Deciphering key features in protein structures with the new ENDscript server. Nucleic Acids Res. 42, W320–W324.
Rusanov, T., Kent, T., Saeed, M., Hoang, T.M., Thomas, C., Rice, C.M., Pomerantz, R.T., 2018. Identification of a small interface between the methyltransferase and RNA polymerase of NS5 that is essential for Zika virus replication. Sci. Rep. 8, 17384.
Sebera, J., Dubankova, A., Sychrovsky, V., Ruzek, D., Boura, E., Nencka, R., 2018. The structural model of Zika virus RNA-dependent RNA polymerase in complex with RNA

for rational design of novel nucleotide inhibitors. Sci. Rep. 8, 11132.
Selisko, B., Papageorgiou, N., Ferron, F., Canard, B., 2018. Structural and functional basis of the fidelity of nucleotide selection by flavivirus RNA-dependent RNA polymerases. Viruses, vol. 10.
Stephen, P., Baz, M., Boivin, G., Lin, S.X., 2016. Structural insight into NS5 of Zika virus leading to the discovery of MTase inhibitors. J. Am. Chem. Soc. 138, 16212–16215.
Upadhyay, A.K., Cyr, M., Longenecker, K., Tripathi, R., Sun, C., Kempf, D.J., 2017. Crystal structure of full-length Zika virus NS5 protein reveals a conformation similar to Japanese encephalitis virus NS5. Acta Crystallogr F Struct Biol Commun 73, 116–122.
Wu, J., Bera, A.K., Kuhn, R.J., Smith, J.L., 2005. Structure of the Flavivirus helicase: implications for catalytic activity, protein interactions, and proteolytic processing. J. Virol. 79, 10268–10277.
Yang, X., Smidansky, E.D., Maksimchuk, K.R., Lum, D., Welch, J.L., Arnold, J.J., Cameron, C.E., Boehr, D.D., 2012. Motif D of viral RNA-dependent RNA polymerases determines efficiency and fidelity of nucleotide addition. Structure 20, 1519–1527.
Zhang, Y., Corver, J., Chipman, P.R., Zhang, W., Pletnev, S.V., Sedlak, D., Baker, T.S., Strauss, J.H., Kuhn, R.J., Rossmann, M.G., 2003. Structures of immature flavivirus particles. EMBO J. 22, 2604–2613.
Zhao, B., Yi, G., Du, F., Chuang, Y.C., Vaughan, R.C., Sankaran, B., Kao, C.C., Li, P., 2017. Structure and function of the Zika virus full-length NS5 protein. Nat. Commun. 8, 14762.
Zhao, Y., Soh, T.S., Zheng, J., Chan, K.W., Phoo, W.W., Lee, C.C., Tay, M.Y., Swaminathan, K., Cornvik, T.C., Lim, S.P., Shi, P.Y., Lescar, J., Vasudevan, S.G., Luo, D., 2015. A crystal structure of the Dengue virus NS5 protein reveals a novel inter-domain interface essential for protein flexibility and virus replication. PLoS Pathog. 11, e1004682.